JACS
JOURNAL OF THE AMERICAN CHEMICAL SOCIETY

ARTICLE

pubs.acs.org/JACS

Formation of a Ruthenium(IV)-Oxo Complex by Electron-Transfer Oxidation of a Coordinatively Saturated Ruthenium(II) Complex and Detection of Oxygen-Rebound Intermediates in C−H Bond Oxygenation

Takahiko Kojima,[*,†] Kazuya Nakayama,[‡] Kenichiro Ikemura,[§] Takashi Ogura,[§] and Shunichi Fukuzumi[*,‡,∥,⊥]

[†]Department of Chemistry, Graduate School of Pure and Applied Sciences, University of Tsukuba, Tennoudai, Tsukuba, Ibaraki 305-8571

[‡]Department of Material and Life Science, Graduate School of Engineering, Osaka University, Japan

[∥]ALCA, Japan Science and Technology Agency (JST), 2-1 Yamada-oka, Suita, Osaka 565-0871, Japan

[§]Graduate School of Life Science, University of Hyogo, Kouto, Hyogo 678-1297, Japan

[⊥]Department of Bioinspired Science, Ewha Womans University, Seoul, South Korea

Supporting Information

ABSTRACT: A coordinatively saturated ruthenium(II) complex having tetradentate tris(2-pyridylmethyl)amine (TPA) and bidentate 2,2′-bipyridine (bpy), $[Ru(TPA)(bpy)]^{2+}$ (**1**), was oxidized by a Ce(IV) ion in H_2O to afford a Ru(IV)-oxo complex, $[Ru(O)(H^+TPA)(bpy)]^{3+}$ (**2**). The crystal structure of the Ru(IV)-oxo complex **2** was determined by X-ray crystallography. In **2**, the TPA ligand partially dissociates to be in a facial tridentate fashion and the uncoordinated pyridine moiety is protonated. The spin state of **2**, which showed paramagnetically shifted NMR signals in the range of 60 to −20 ppm, was determined to be an intermediate spin ($S = 1$) by the Evans' method with ^{1}H NMR spectroscopy in acetone-d_6. The reaction of **2** with various oraganic substrates in acetonitrile at room temperature afforded oxidized and oxygenated products and a solvent-bound complex, $[Ru(H^+TPA)(bpy)(CH_3CN)]$, which is intact in the presence of alcohols. The oxygenation reaction of saturated C−H bonds with **2** proceeds by two-step processes: the hydrogen abstraction with **2**, followed by the dissociation of the alcohol products from the oxygen-rebound complexes, Ru(III)-alkoxo complexes, which were successfully detected by ESI-MS spectrometry. The kinetic isotope effects in the first step for the reaction of dihydroanthrathene (DHA) and cumene with **2** were determined to be 49 and 12, respectively. The second-order rate constants of C−H oxygenation in the first step exhibited a linear correlation with bond dissociation energies of the C−H bond cleavage.

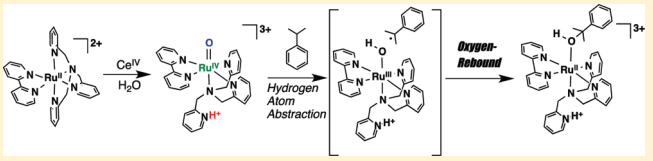

INTRODUCTION

High-valent metal−oxo complexes are known to act as reactive species for oxidation of various substrates in both biological and chemical systems.[1−3] Extensive efforts have so far been devoted to understand the structures and reactivities of high-valent metal−oxo complexes, which have normally been produced by reactions of metal complexes with active oxygen species such as iodosylbenzene (PhIO), *m*-chloroperbenzoic acid (*m*-CPBA), and hydroperoxides (H_2O_2 and ROOH), or with O_2 in the presence of electron and proton donors.[4−8] To promote those reactions, it is required for the metal complexes to have a vacant site or a labile ligand such as a solvent molecule or halides to accommodate the coordination of the oxidant for its activation. Alternatively, high-valent metal−oxo intermediates have been produced by the two-electron oxidation of metal complexes with water as an oxygen source for the oxo ligand.[9−11] In this process, aqua complexes having a water molecule as a ligand have been required to be oxidized via proton-coupled electron transfer to afford the high-valent metal−oxo complexes.

Thus, although being the majority of coordination compounds, coordinatively saturated metal complexes in which all the coordination sites are occupied by chelating ligands have been excluded as precursor complexes to afford high-valent metal−oxo complexes. However, if high-valent metal−oxo complexes can be formed using coordinatively saturated metal complexes, the possibility will be widely expanded in application of metal complexes to form high-valent metal−oxo species as responsible intermediates in substrate oxidations. As a strategy to make it possible to apply coordinatively saturated metal complexes to oxidation reactions involving the generation of high-valent metal−oxo complexes, structural change such as partial ligand dissociation is required in the course of the reaction to

Received: April 24, 2011
Published: June 22, 2011

dx.doi.org/10.1021/ja2037645 | *J. Am. Chem. Soc.* 2011, 133, 11692–11700

Scheme 1

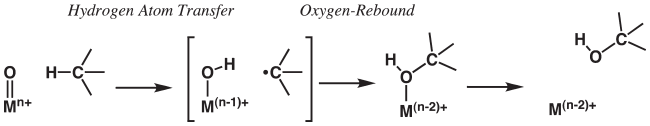

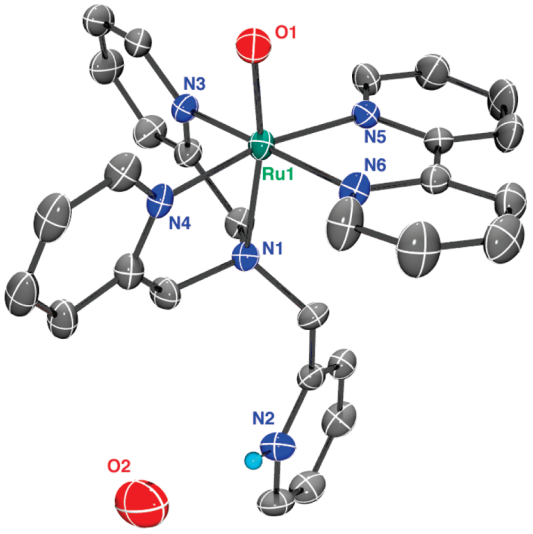

Figure 1. ORTEP drawing of the cation moiety of **2** using 50% probability thermal ellipsoids with numbering scheme for the heteroatoms. Hydrogen atoms are omitted for clarity except the hydrogen on the uncoordinated pyridine nitrogen (N2). O2 represents the water molecule of crystallization. Selected bond lengths (Å): Ru1−O1 1.771(4), Ru1−N1 2.242(4), Ru1−N2 2.083(4), Ru1−N4 2.072(4), Ru1−N5 2.070(4), Ru1−N6 2.073(4).

accommodate a coordination site for the formation of the oxo ligand. However, there has so far been no report on generation of high-valent metal−oxo complexes starting from coordinatively saturated metal complexes through proton-coupled electron transfer.

High-valent metal−oxo complexes are capable of hydroxylation of a C−H bond, which has been believed to proceed via an "oxygen-rebound" mechanism as shown in Scheme 1.[12] Hydrogen atom transfer from substrates to high-valent metal−oxo complexes affords the hydrogen abstracted radicals and the hydoxo complexes, followed by oxygen-rebound between them to produce the corresponding alcohols. Although much effort has been devoted to gain mechanistic insights into proving the rebound mechanism by experiments[13] as well as calculations,[14] direct observation of the oxygen-rebound intermediates has yet to be achieved.[15−17]

We report herein the first example of generation of a high-valent metal−oxo complex using a coordinatively saturated metal complex, which is stabilized by two chelating ligands without aqua ligand. The electron-transfer oxidation of a hexacoordinated ruthenium(II) complex having tris(2-pyridylmethyl)amine (TPA) and 2,2′-bipyridine (bpy) as chelating ligands, $[Ru(TPA)(bpy)]^{2+}$ (**1**),[18] with a Ce(IV) ion afforded the corresponding Ru(IV)−oxo complex, $[Ru(O)(H^{+}TPA)(bpy)]^{3+}$ (**2**). Successful isolation and determination of the crystal structure of **2** have allowed us to examine the mechanism of the C−H bond activation with **2** including the first direct

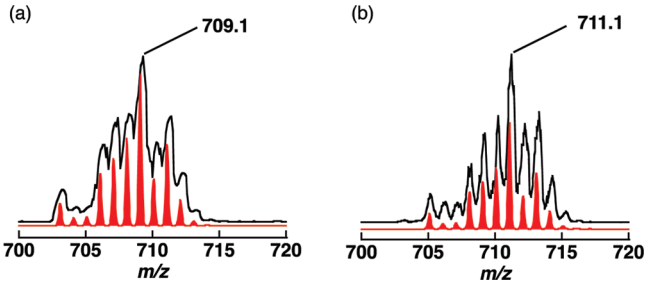

Figure 2. Positive-ion ESI-MS spectra of **2** in CH_3CN. (a) Peak cluster at m/z 709.1 assigned to $\{\mathbf{2} - H^{+} - 2(PF_6^{-})\}^{+}$; (b) peak cluster at m/z = 711.1 assigned to $\{\mathbf{2}(^{18}\mathbf{O}) - H^{+} - 2(PF_6^{-})\}^{+}$. Red lines show the computer-simulated isotope patterns.

observation of the oxygen-rebound process in the course of hydroxylation of saturated C−H bonds.

RESULTS AND DISCUSSION

Characterization of a Ruthenium(IV)−Oxo Complex. A Ru(II) complex, $[Ru(TPA)(bpy)](PF_6)_2$ (**1**),[18] having a tetradentate ligand of TPA and a bidentate ligand of bpy as ligands was oxidized by $(NH_4)_2[Ce^{IV}(NO_3)_6]$ (CAN) in H_2O at room temperature. In the UV−vis spectrum, the MLCT band peculiar to **1** disappeared by the addition of CAN to an aqueous solution of **1** (see Figure S1 in Supporting Information). The reaction afforded a light-green complex **2** and its crystal structure was determined by X-ray crystallography. The crystal structure of the cation part of **2** is depicted in Figure 1 with a partial numbering scheme.[19] The light-green complex was revealed to be a Ru(IV)−oxo complex, $[Ru(O)(H^{+}TPA)(bpy)](PF_6)_3$ (**2**), bearing an oxo ligand, the bpy ligand, and a protonated TPA ligand ($H^{+}TPA$) in a facial and tridentate coordination mode. In the course of the formation of **2**, the complex was revealed to undergo structural change, which is reminiscent of the photochromic behavior of **1**,[18] in terms of the coordination mode of the TPA ligand involving its partial dissociation. The bond length of Ru−O bond is 1.771(4) Å, which is in the range of those of Ru(IV)−oxo bonds reported so far.[20] The uncoordinated pyridine moiety is protonated and the proton attached to the pyridine nitrogen atom forms a hydrogen bond with a water molecule of crystallization and one of fluorine atoms of PF_6^{-} (N2···O2: 2.738(8) Å, N2···F: 2.899(6) Å).

ESI-MS spectrometry was applied to detect the signal due to $\{\mathbf{2} - H^{+} - 2(PF_6^{-})\}^{+}$ at m/z = 709.1 in CH_3CN prepared in $H_2{}^{16}O$, and the mass number was shifted to m/z = 711.1 for the sample prepared in $H_2{}^{18}O$ as shown in Figure 2. These results indicate that the Ru(IV)−oxo complex **2** is stable in solution to maintain the oxo ligand and that the oxo-oxygen comes from water.

The Ru(IV)-oxo complex **2** showed paramagnetically shifted NMR signals in the range of 60 to −20 ppm, and the spin state was determined to be an intermediate spin (S = 1) by the Evans' method[21] with ^{1}H NMR spectroscopy in acetone-d_6 (see Figure S2 in Supporting Information).

The resonance Raman spectrum of **2** prepared in $H_2{}^{16}O$ was measured by the laser excitation at 363.8 nm with an Ar^{+} laser. A peak obsreved at 805 cm^{-1} was assigned to the Raman scattering of the Ru=O moiety (ν(Ru=O)), which shifted to 764 cm^{-1} when **2** was prepared in $H_2{}^{18}O$ as shown in Figure 3. The shift

dx.doi.org/10.1021/ja2037645 |J. Am. Chem. Soc. 2011, 133, 11692–11700

value ($\Delta\nu = 41\ cm^{-1}$) agrees with the calculated value ($\Delta\nu_{calcd} = 40\ cm^{-1}$) for ν(Ru═O). The Raman shift of the ν(Ru═O) for **2** is comparable to that ($805\ cm^{-1}$) observed for $[Ru^{IV}(O)(TPA)(OH_2)]^{2+}$ in the intermediate spin state[10a] and falls in the lower range of those of Ru^{IV}═O bonds.[20a,22]

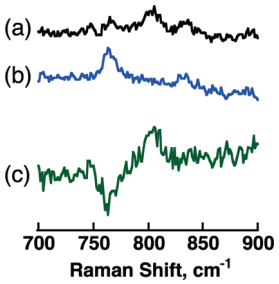

Figure 3. Resonance Raman spectra of **2** in (a) $H_2{}^{16}O$ and (b) $H_2{}^{18}O$. (c) Differential spectrum of ($^{16}O - {}^{18}O$).

The one-electron reduction potential of **2** was determined to be 0.70 V (versus SCE) by SHACV (second harmonic ac voltammetry) in the presence of 0.1 M of $[(n\text{-butyl})_4N]PF_6$ as an electrolyte in CH_3CN at room temperature under Ar and 0.80 V (vs SCE) by SHACV in the presence of 0.1 M of Na_2SO_4 as an electrolyte at pH = 1 adjusted by aqueous H_2SO_4 at room temperature under Ar (see Figure S3 in Supporting Information). This potential is comparable to those of Ru^{IV}/Ru^{III} redox couples for $[Ru^{IV}(O)(TPA)(H_2O)]^{2+}$ (0.74 V)[10a] and $[Ru^{IV}(6\text{-}COO^{-}\text{-}TPA)(O)(H_2O)]^{+}$ (0.68 V)[10b] in a Britton-Robinson buffer at pH = 2.

Oxidation Reactions of Organic Substrates by 2 Involving Hydrogen Abstraction. The complex **2** was employed for oxidation of various organic substrates in CH_3CN at room temperature. Substrates used and their bond dissociation energies (BDEs), methods, products and their yields are summarized in Table 1. When 10-methyl-9,10-dihydroacridine (entry 1) was used as a substrate, the two-electron oxidized product

Table 1. Yields of Products in Oxidation of Various Substrates by 2 (5 mM) in Acetonitrile under Inert Atmosphere at Room Temperature

entry	substrate	E_{ox} vs SCE (V)	BDE (kcal/mol)[a]	[sub] (mM)	product (yield %)	ox. eff. (%)[b]
1	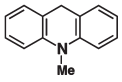	0.81[c]	73.7	10	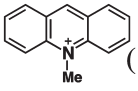 (100)[w]	100
2	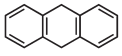	1.62[d]	76.3	50	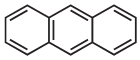 (20)[x] 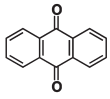 (18)[x]	92
3	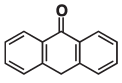	-	80.2	50	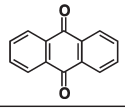 (46)[x]	92
4		1.73[e]	81.6	50	 (44)[w]  (5)[w]	93
5	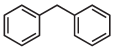	1.91[f]	84.5	50	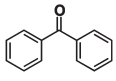 (18)[w] 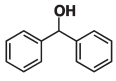 (12)[w]	48
6		2.14[c]	84.8	50	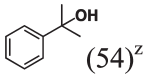 (54)[z]  (6)[z]  (6)[z]	72
7	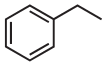	2.14[c]	85.4	100	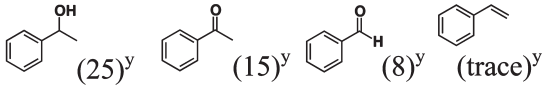 (25)[y] (15)[y] (8)[y] (trace)[y]	71
8		2.20[c]	88.5	500	 (23)[y]	46

[a] Adapted from ref 23. [b] Oxidation efficiency (%) = [{[Product(s)]/(2 × [**2**])} × N(oxidation equivalent)] × 100. [c] Adapted from ref 24. [d] Adapted from ref 25. [e] Adapted from ref 26. [f] Adapted from ref 27. Methods: w, by NMR in CD_3CN; x, by NMR in $CDCl_3$; y, by GC-MS in CH_3CN; z, by NMR and GC-MS in CD_3CN (w−y, 1,4-cyclohexadione as an internal reference; z, methoxybenzene as internal references). Product yields are based on **2**.

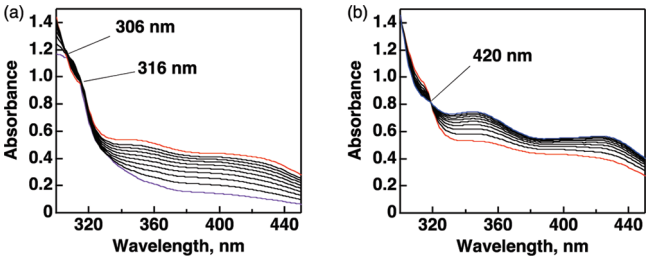

Figure 4. Absorption spectral change in the course of the reaction of **2** (0.1 mM) with cumene (200 mM) in CH_3CN under Ar at 298 K: (a) 0−650 s; (b) 650−3000 s.

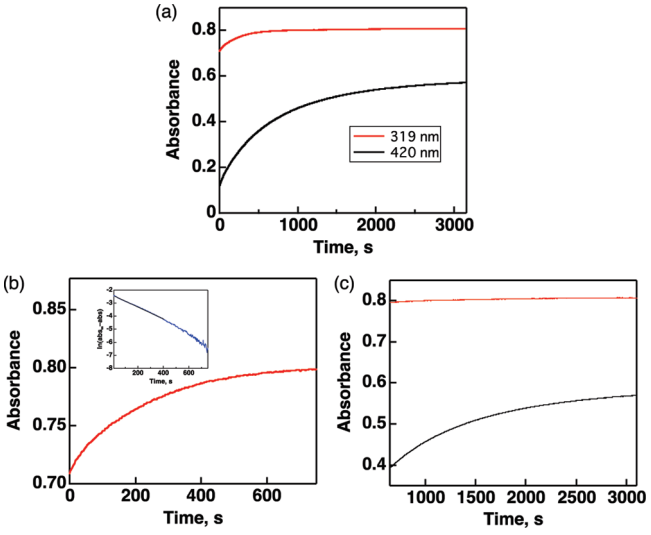

Figure 5. Absorbance change at 319 nm (red line) and 420 nm (black line) in the course of the reaction of **2** (0.1 mM) with cumene (200 mM) in CH_3CN under Ar at 298 K: (a) 0−3200 s; (b) 0−650 s (the first step); (c) 650−3000 s (the second step).

(10-methylacridinium ion) was obtained in 100% yield. 9, 10-Dihydroanthracene (DHA; entry 2) was converted to the two-electron oxidized product, anthracene (20%), and the eight-electron oxidized product, anthraquinone (18%). 9-Oxo-10-hydroanthracene (anthrone, entry 3) was converted to the four-electron oxidized product, anthraquinone (46%). Cyclohexene (entry 4) was also oxidized to the four-electron oxidized product, cyclohexene-1-one (44%), and the two-electron oxidized product, cyclohexen-1-ol (5%). The overall oxidant efficiency of these substrates, which have lower BDE values than 82 kcal mol^{-1}, with **2** is higher than 90%. Diphenylmethane (entry 5) was converted to benzophenone (18%) and diphenylmethanol (12%). The lower oxidant efficiency should stem from steric hindrance in the access of bulky diphenylmethane to the oxo ligand. Cumene (entry 6) was also converted to the two-electron oxidized product, 2-phenyl-2-propanol (cumyl alcohol: 54%), α-methylstyrene (6%), and the four-electron oxidized product, acetophenone (6%), when the overall oxidation efficiency is 72%. Ethylbenzene (entry 7) underwent benzylic oxygenation to yield the two-electron oxidized product, benzyl alcohol (25%) and styrene (trace), and the four-electron oxidized products, acetophenone (15%) and benzaldehyde (8%) with the overall oxidation efficiency of 81%. Toluene (entry 8) was also oxygenated to yield the four-electron oxidized product, benzaldehyde

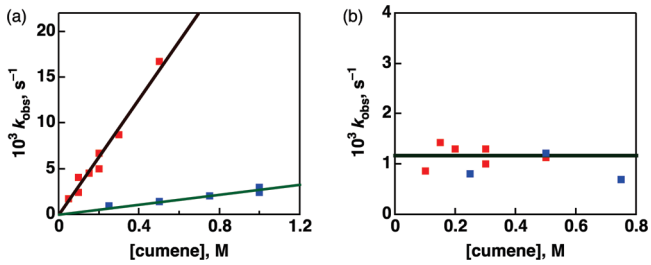

Figure 6. (a) Concentration dependence of pseudo-first-order rate constants for the first step of the reaction of **2** with cumene in CH_3CN at 298 K: red, cumene; blue, cumene-d_{12}. (b) Concentration dependence of pseudo-first-order rate constants for the second step of reaction of **2** with cumene in CH_3CN at 298 K: red, cumene; blue, cumene-d_{12}.

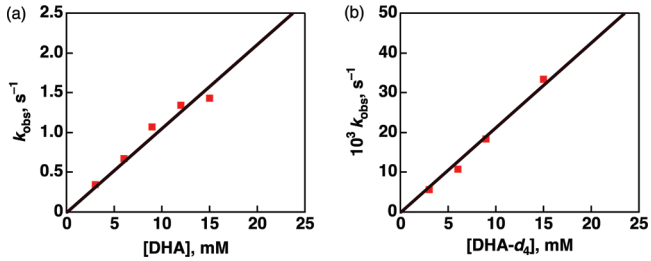

Figure 7. Concentration dependence of pseudo-first-order rate constants for the reaction of **2** with (a) DHA and (b) DHA-d_4 in CH_3CN at 298 K.

(23%) with the overall oxidation efficiency of 46%. The low oxidation efficiency for toluene may stem from its high BDE value (88.5 kcal mol^{-1}) compared to that of O−H bond formed by the hydrogen abstraction by **2**.

Kinetic Analysis of Reaction Mechanisms. To obtain the mechanistic insight into the oxidation of substrates with **2**, we conducted the kinetic analysis in deaerated CH_3CN using UV−vis spectroscopy. The absorption spectrum of **2** in the reaction with cumene exhibited a two-step spectral change as shown in Figure 4a and b. In the first step up to 650 s after mixing, the spectral change was observed as an increase in a broad absorption band ranging from 330 to 450 nm with isosbestic points at 306 and 316 nm (Figure 4a). The time profile of the absorption change obeyed pseudo-first-order kinetics as shown in Figure 5. The pseudo-first-order rate constant (k_{obs}) increased linearly with increasing cumene concentration (red squares in Figure 6a). The second-order rate constant (k_1) for the first step was determined from the slope of the linear plot in Figure 6a to be $(3.2 \pm 0.1) \times 10^{-2}$ M^{-1} s^{-1}. Virtually the same value $[(3.3 \pm 0.1) \times 10^{-2}$ M^{-1} $s^{-1}]$ was obtained under O_2 (see Figure S4 in Supporting Information).

When cumene was replaced by the corresponding deuterated compound (cumene-d_{12}), the second-order rate constant was determined to be $(2.74 \pm 0.14) \times 10^{-3}$ M^{-1} s^{-1} (blue points in Figure 6a), which is significantly smaller that the value of cumene. From the rate constants of cumene and cumene-d_{12}, the kinetic isotope effect (KIE) was determined to be 12 for the first step of the cumene oxygenation.

The oxidation of 9,10-dihydroanthracene (DHA) and the deuterated compound (DHA-d_4) with **2** also proceeded by the two steps. The pseudo-first-order rate constant increased linearly with increasing DHA concentration as shown in Figure 7.

dx.doi.org/10.1021/ja2037645 |*J. Am. Chem. Soc.* 2011, 133, 11692–11700

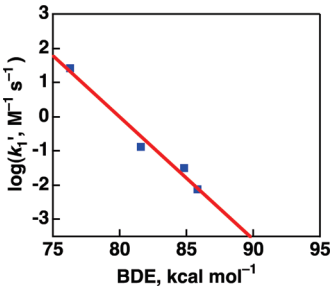

Figure 8. Plot of logk_1' vs BDEs of substrates for oxidation of substrates with **2** in CH_3CN at 298 K.

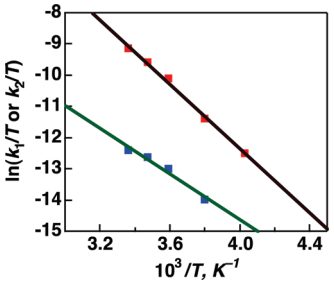

Figure 9. Eyring plots for the oxidation of cumene with **2** (red: the first step (k_1, M^{-1} s^{-1}); blue: the second step (k_2, s^{-1})).

The second-order rate constants for the first step in the oxidation of DHA and DHA-d_4 with **2** were determined to be (1.05 ± 0.05) × 10^2 M^{-1} s^{-1} and 2.13 ± 0.09 M^{-1} s^{-1}, respectively, from which the KIE value was determined to be 49. In this case, the hydrogen atom transfer probably occurs via proton-coupled electron transfer with tunneling.[28] The large KIE value indicates that the first step should be the hydrogen abstraction from substrates by **2**.

The second-order rate constants for the first step in the oxidation of other substrates were also determined from plots of the observed pseudo-first-order rate constant vs concentration of substrates (see Figure S5 in Supporting Information for an example of the case of ethylbenzene). The logarithm of the normalized second-order rate constants (k_1') for the first step in oxidation of various substrates by **2** exhibited a linear relationship with the bond dissociation energies of the C−H bond of the corresponding substrates as shown in Figure 8, where the observed second-order rate constants are divided by the number of equivalent hydrogen atoms to be abstracted at the same position to obtain k_1'.[29,30] The linear correlation between log k_1' and BDE in Figure 8 strongly indicates that the hydrogen atom abstraction occurs in a common mechanism for all the investigated substrates.[11b,30]

The spectral change in the second step at later than 650 s after mixing of cumene with **2** is shown in Figure 3b, where a new isosbestic point is observed at 319 nm. The rate of the second step also obeyed first-order kinetics. The first-order rate constants (k_2) of the second step in the oxygenation of cumene, cyclohexene, and ethybenzene were determined to be 1.17, 1.03, and 1.09 s^{-1}, respectively. In contrast to the case of the first step (Figure 5a), the observed first-order rate constant shows no dependence on the substrate concentration as shown in Figure 5b and Figure 6 (blue points). The temperature dependence of the rate constants of the first and the second steps in the

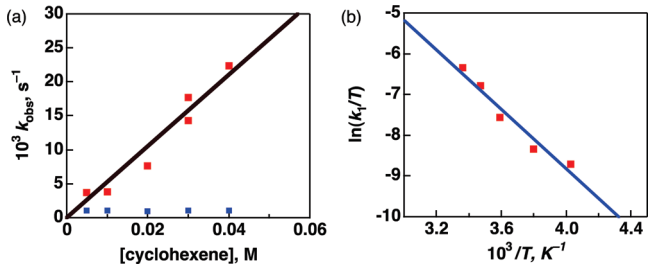

Figure 10. (a) Concentration dependence of pseudo-first-order rate constants of reaction of **2** with cyclohexene in CH_3CN at 298 K: red, the first step; blue, the second step. (b) Eyring plot for the second-order rate constants of the first step (k_1, M^{-1} s^{-1}) in the reaction of **2** with cyclohexene.

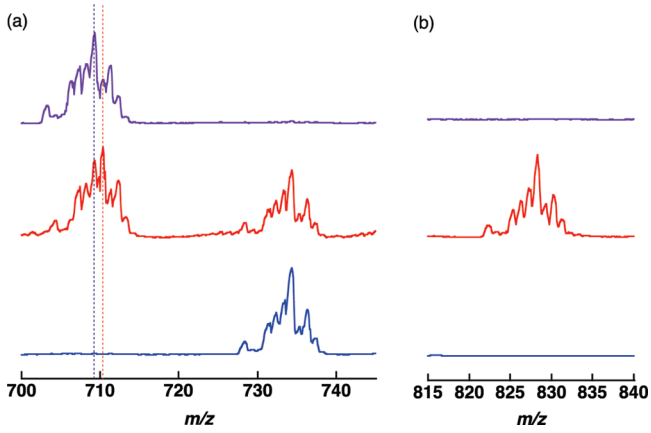

Figure 11. Time-course of ESI-MS spectra of the reaction mixture of **2** (0.1 mM) and cumene (200 mM) in CH_3CN (purple line: 0 min, red line: 15 min, blue line; 300 min). (a) Range, m/z = 700−745; (b) range, m/z = 815−840.

oxidation of cumene with **2** in CH_3CN are compared in the Eyring plots (Figure 9). The activation parameters of the first step was determined to be $\Delta H^{\ddagger}$ = 10 ± 0.40 kcal mol^{-1} and $\Delta S^{\ddagger}$ = −31 ± 1.5 cal mol^{-1} K^{-1}. The activation enthalpy of the second step ($\Delta H^{\ddagger}$ = 7.3 ± 0.9 kcal mol^{-1}) is smaller than the value of the first step ($\Delta H^{\ddagger}$ = 10 ± 0.40 kcal mol^{-1}), whereas the activation entropy ($\Delta S^{\ddagger}$ = −47 ± 3.1 cal mol^{-1} K^{-1}) is more negative than the value of the first step ($\Delta S^{\ddagger}$ = −31 ± 1.5 cal mol^{-1} K^{-1}).

The activation parameters for the first step in the oxidation of cyclohexene with **2** to give cyclohexene-1-one (entry 4 in Table 1) were also determined to be $\Delta H^{\ddagger}$ = 7.2 ± 1.0 kcal mol^{-1} and $\Delta S^{\ddagger}$ = −36 ± 3.5 cal mol^{-1} K^{-1} as shown in Figure 10. These values are virtually identical with those obtained in the reaction of the same substrate (cyclohexene) with $[Ru^{IV}(O)(bpy)_2(py)]^{2+}$ ($\Delta H^{\ddagger}$ = 7.4 ± 0.1 kcal mol^{-1} and $\Delta S^{\ddagger}$ = −34 ± 3.4 cal mol^{-1} K^{-1}).[31] The identical reactivity of **2** may result from the nearly the same one-electron reduction potential of **2** (0.80 V at pH = 1 in water) as that of $[Ru^{IV}(O)(bpy)_2(py)]^{2+}$ (0.85 V at pH = 1 in water).[32]

Detection of Intermediates in Substrate Oxygenation Reactions. ESI-MS spectrometry was applied in order to detect intermediates in the two-step processes for the oxidation of substrates with **2** in CH_3CN, In the course of the reaction of **2** ($\{2 - H^+ - 2(PF_6^-)\}^+$, m/z = 709.1) with cumene in CH_3CN

at room temperature, signals due to a Ru(III)-hydroxo complex $[Ru^{III}(OH)(H^+TPA)(bpy)]^{2+}$ (**3**) ($\{3 - H^+\}^+$, m/z = 710.1) and a Ru(III)-cumyl alkoxo complex, $[Ru^{III}(OC(CH_3)_2(C_6H_5))(H^+TPA)(bpy)]^{2+}$(**4**) ($\{4 - H^+\}^+$, m/z = 828.2) were observed as shown in Figure 11 (see also Figure S6 in Supporting Information). The isotope patterns agree with those obtained by computer simulations (Figure S7 in Supporting Information). When the ^{18}O-labeled complex, $[Ru(^{18}O)(H^+TPA)(bpy)](PF_6)_3$ (**2**-^{18}O), was employed as the starting material, the signals due to **3** and **4** were shifted to m/z = 712.1 and m/z = 830.2, respectively (Figure 12). Formation of Ru(III)−alkoxo complexes was also observed in the reactions of **2** with cyclohexene, dihydroanthracene,[33] anthrone, ethylbenzene, and diphenylmethane (Figures S8−12 in Supporting Information). All the alkoxo complexes were finally converted to $[Ru^{II}(H^+TPA)(bpy)(CH_3CN)]^{3+}$ (**5**) ($\{5 - H^+\}^+$, m/z = 734.1) at the end of the reaction (blue line in Figure 11a).

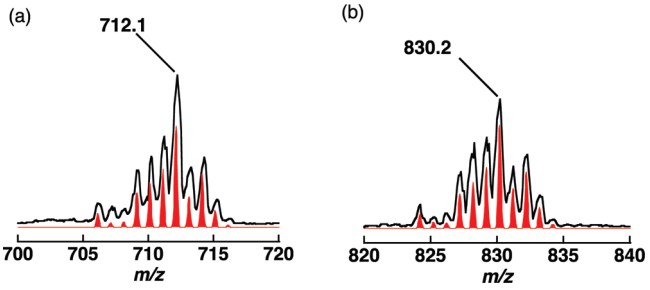

Figure 12. ESI-MS spectra of the mixture of cumene (200 mM) and **2**(^{18}O) (0.1 mM) in CH_3CN. (a) Peak cluster at m/z = 712.1 assigned to $\{3(^{18}O) - H^+\}^+$; (b) peak cluster at m/z = 830.2 assigned to $\{4(^{18}O) - H^+\}^+$.

The Ru(III)−hydroxo complex **3** and the Ru(III)-alkoxo complex **4** may be formed via the oxygen-rebound reaction as shown in Scheme 2 in the case of oxidation of cumene with **2**. The complex **1** is rapidly oxidized with CAN with water as an oxygen source to afford **2**. In the first step, hydrogen atom transfer from cumene to **2** occurs to produce cumyl radical and the Ru(III)−hydroxo complex **3**. The oxygen rebound between cumyl radical and **3** affords the Ru(II)-alcohol complex. The Ru(II)−alcohol complex may be readily oxidized by **2** via hydrogen atom transfer to produce **3** and the Ru(III)−alkoxo complex **4**. The formation of Ru(III) complexes **3** and **4** in the reaction of **2** with cumene in CH_3CN detected by ESI-MS spectra in Figure 11 was confirmed by the EPR spectroscopic measurements at 8 K as shown in Figure 13. The observed EPR signal at g = 1.89, 2.16, and 2.40 in Figure 13 is typical for Ru(III) complexes.[34] The reverse reaction may also occur to reproduce the Ru(II)−cumyl alcohol complex, which slowly dissociates by ligand substitution with CH_3CN to yield $[Ru^{II}(H^+TPA)(bpy)(CH_3CN)]^{3+}$ (**5**) and cumyl alcohol as the final products. As mentioned above, the negative activation entropy for the second step in the oxygenation of cumene indicates that this ligand substitution process proceeds via an associative mechanism as observed in thermal ligand dissociation in **1** to afford **5**.[18b] Complex **5** in the presence of large excess cumyl alcohol was not converted to $[Ru^{II}(H^+TPA)(bpy)(cumyl\ alcohol)]^{3+}$, due to strong interaction of CH_3CN with the Ru(II) center.[35] Also, cumyl alcohol is not oxidized by **2** under the same reaction

Scheme 2

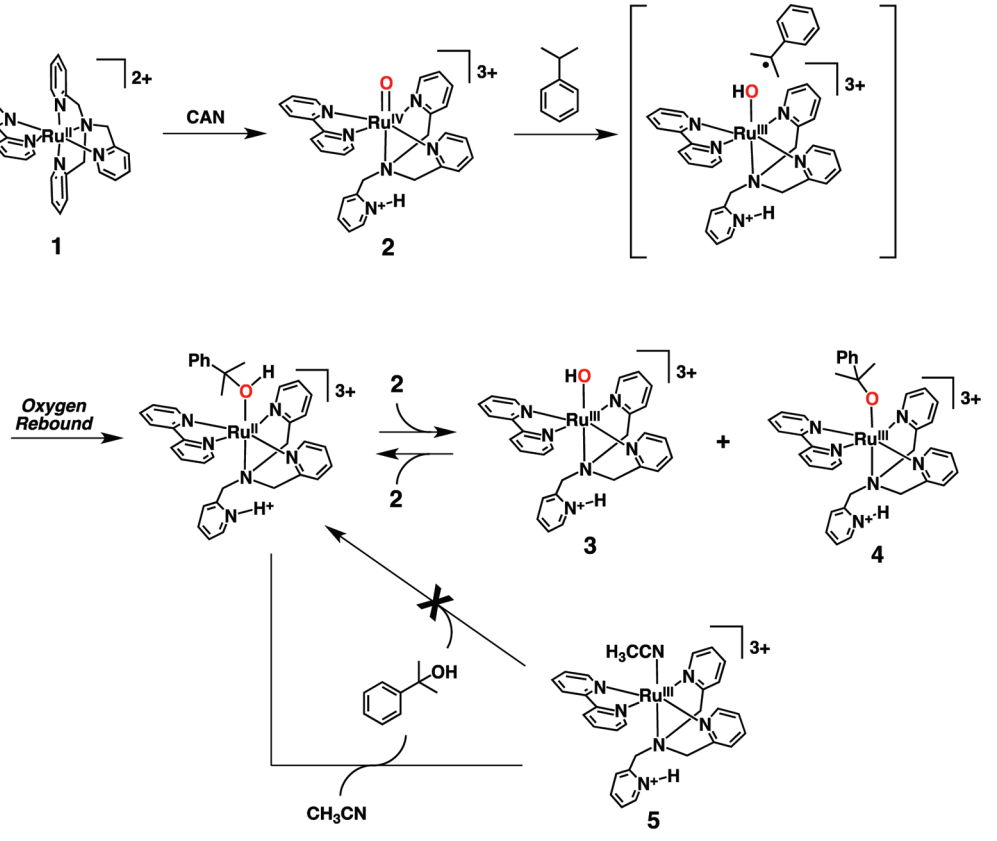

dx.doi.org/10.1021/ja2037645 |J. Am. Chem. Soc. 2011, 133, 11692–11700

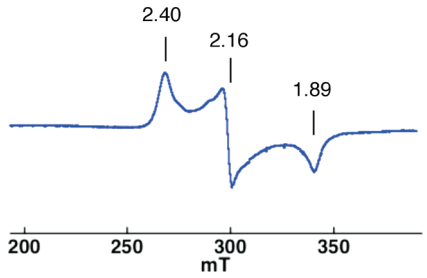

Figure 13. EPR spectrum of the reaction mixture of **2** and cumene in CH_3CN at 8 K.

conditions due to the stronger O−H bond than the tertiary C−H bond in cumene.[36]

According to Scheme 2, the first step corresponds to the hydrogen abstraction from cumene by **2** to produce the Ru(II)−cumyl alcohol complex, when the rate is proportional to concentration of cumene with the large kinetic isotope effect. The second step corresponds to the ligand displacement of the Ru(II)−cumyl alcohol complex by CH_3CN to release cumyl alcohol, which competes with the oxidation by **2** to produce **3** and **4**, which were detected as intermediates by ESI-MS. The equilibrium between the hydrogen atom transfer from Ru(II)−cumyl alcohol complex to **2** and the backward hydrogen atom transfer from **3** to **4** in Scheme 2 lies to the right side (**3** and **4**), because only **3** and **4** were detected by ESI-MS. As the ligand substitution of the Ru(II)−cumyl alcohol complex proceeds in the second step, **3** and **4** are converted to **5**. Because the rate-determining step in the second step involved no reaction with cumene and hydrogen abstraction, the rate is independent of cumene concentration with no kinetic isotope effect (Figure 5b) and regardless of deuterium substitution of the alcohol O−H group by addition of excess amount of D_2O (2 M) (Figure S13 in Supporting Information). In addition, since the complex **5** is intact in the presence of excess amount of cumyl alcohol, it cannot be a precursor to afford the Ru(II)−cumyl alcohol complex.

Mayer and co-workers have previously reported the trapping of radical species by O_2 in the cumene oxygenation by $[Ru^{IV}(O)(bpy)_2(py)]^{2+}$ in CH_3CN.[37] In our case, however, no effect of O_2 was observed on the rate of the reaction of **2** with cumene (vide supra). The products also remained the same in the presence of O_2 as those in the absence of O_2. In addition, no organic radical was detected by EPR measurements in Figure 13. Moreover, the addition of CH_2Br_2 or CBr_4 used as radical traps resulted in no effect on the product distribution without forming any brominated products.[38] Thus, we concluded that the nascent radical species formed by the hydrogen abstraction is not released from a solvent cage and resides in the second coordination sphere to undergo a fast oxygen-rebound reaction.[39,40]

SUMMARY AND CONCLUSION

We have synthesized an intermediate-spin ($S = 1$) Ru(IV)-oxo complex from a coordinatively saturated Ru(II) complex without aqua ligand via structural change involving partial dissociation of a multidentate ligand, followed by proton-coupled electron transfer. The Ru(IV)−oxo complex was characterized by crystallographic, spectroscopic, and electrochemical methods. We have succeeded in the direct observation of "oxygen-rebound" process in the course of hydroxylation of a saturated C−H bond by the Ru(IV)−oxo complex by using ESI-MS spectrometry. This is the first example of the direct observation of "oxygen-rebound" process, which has been proposed as a fundamental reaction mechanism for hydroxylation of C−H bond by high-valent metal−oxo complexes. The hydrogen atom abstraction by **2** proceeds via a compact and well-ordered transition state as demonstrated by the activation parameters and with large KIE values.

EXPERIMENTAL SECTION

Materials. $(NH_4)_2[Ce^{IV}(NO_3)_6]$ (CAN) was used as received and its purity was determined to be 67% by iodometry. CH_3CN was used after distillation over CaH_2. All other solvents were of special grade and were used as received from commercial sources without further purification. TPA·$3HClO_4$,[41] $[RuCl(TPA)]_2(ClO_4)_2$,[42] $[Ru(TPA)(bpy)](PF_6)_2$[18] were synthesized as reported previously. Cyclohexene was purified by passage through a column of alumina to remove the BHT stabilizer. Dihydroanthracene (DHA) was recrystallized twice from absolute ethanol.

Instrumentation. UV−vis spectra were recorded on a Hewlett-Packard HP8453 photodiode array spectrophotometer. ^1H NMR spectra were recorded on a JEOL JMN-AL-300 NMR spectrometer at room temperature. Electrochemical measurements were carried out using a BAS 100W electrochemical analyzer. Gas chromatographic analyses were performed on a Shimadzu GC-17A equipped with DB-5 ms (Agilent J&W, 30 m) or Inertcap 5 ms/sil column (GL Science, 30 m) and a mass spectrometer (Shimadzu QP 5000) as a detector. ESI-MS spectra were recorded on a Perkin-Elmer API-150 spectrometer. Stopped-flow measurements were performed with a UNISOKU RSP-601 stopped-flow spectrophotometer with an MOS-type high selective photodiode array. EPR spectra were recorded on a JEOL JEXREIXE spectrometer, and g values were determined using an Mn^{2+} marker.

$[Ru^{IV}(O)(H^+TPA)(bpy)](PF_6)_3$ (2). $[Ru(TPA)(bpy)](PF_6)_2$ (25 mg, 30 mmol) were added to a solution of $(NH_4)_2[Ce^{IV}(NO_3)_6]$ (65 mg 79 mmol) in water (3 mL) and stirred vigorously for several minutes. When the orange power of $[Ru(TPA)(bpy)](PF_6)_2$ dissolved, light green solution was obtained. KPF_6 (50 mg 270 mmol) were added to afford light-green powder. The light-green precipitate was washed with small amount of ether and then dried (24 mg. Yield: 83%). Anal. Calcd for $C_{28}H_{27}ON_6P_3F_{18}Ru$: C, 33.65; H, 2.72; N, 8.41. Found: C, 33.42; H, 2.70; N, 8.45. ESI-MS: 709.1 ($\{M - PF_6\}^+$).

Resonance Raman Spectroscopy. Samples were prepared under following conditions. For $[Ru(^{16}O)(H^+TPA)(bpy)]^{3+}$: To a 1 mL of $H_2{}^{16}O$ solution of $[Ru(TPA)(bpy)](PF_6)_2$ (1.7 mg, 2.0 μmol) was added a CAN (4.4 mg, 8.0 μmol) and stirred for 2 min. For $[Ru(^{18}O)(H^+TPA)(bpy)]^{3+}$: To a 120 μL of $H_2{}^{18}O$ solution of $[Ru(TPA)(bpy)](PF_6)_2$ (0.3 mg, 0.36 μmol) was added a CAN (2.2 mg, 4.0 μmol) and stirred for 2 min. Resonance Raman scattering was made by excitation at 363.8 nm with an Ar^+ laser (Spectra Physics, 2080−25/2580C), dispersed by a single polychromator (Ritsu Oyo Kogaku, MC-100DG) and detected by a liquid-nitrogen-cooled CCD detector (Roper Scientific, LNCCD-1100-PB). The resonance Raman measurements were carried out at 22 °C using a spinning cell (outer diameter = 3 mm, wall thickness = 1 mm) at 90° scattering geometry.

X-Ray Crystallography on 2. A single crystal of **2** was obtained by standing a mixture of $[Ru(TPA)(bpy)](PF_6)_2$ and CAN overnight in water at room temperature. The crystals were mounted on a glass capillary with epoxy resin. All measurements were performed on a Rigaku Mercury CCD diffractometer at −150 °C with a graphite-monochromated Mo Kα radiation ($\lambda = 0.71073$ Å). The data were collected up to $2\theta = 55.0°$. The structure was solved by direct methods and expanded using Fourier techniques. All non-hydrogen atoms were refined anisotropically. Refinement was carried out with full-matrix least-squares on F with scattering factors[43] and including anomalous dispersion effects.[44] All calculations

were performed using the Crystal Structure crystallographic software package,[45] and structure refinements were made by using SHELX-97.[46,47]

General Procedure for Oxygenation Reactions. A solution was prepared in 0.6 mL of CD_3CN to contain 3 μmol of **2** and fixed amount of 1,4-cyclohexadione or methoxybenzene as an internal standard for NMR and GC-MS quantification. To the solution, 0.006−0.3 mmol of a substrate was added and the mixture was stirred at room temperature at least 120 min. ESI-MS measurements were performed to clarify the end of reaction. The solution was directly analyzed by ^{1}H NMR spectroscopy and GC-MS analysis to obtain quantitative data for the products. All reactions were conducted in an inert atmosphere.

Kinetic Studies. All kinetic experiments on the oxidation of ethylbenzene, cumene and cyclohexene were performed using a photodiode array with 1 cm cell in acetonitrile and oxidation of dihydroanthracene was performed on a UNISOKU RSP-601 stopped-flow spectrometer equipped with a MOS-type highly sensitive photodiode array or a Hewlett-Packard 8453 photodiode-array spectrophotometer at 298 K in acetonitrile. The reactions were monitored by absorbance changes at 318 or 319 nm for the first step and 420 nm for the second step. The rate constants in the first step were determined from the gradient of the plot of $\ln(A-A_\infty)$ at 318 or 319 nm vs time, where A_∞ was the absorbance at 318 or 319 nm at the end of the first reaction. The rate constants in the second step were determined by using the fitting equation as follows: $f(t) = a + b(1 - \exp(-k_{obs}t))$, where $f(t)$ was absorbance at 420 nm at certain time (t sec), k_{obs} was the first-order rate constant in the second step; a and b were coefficients. The initial concentrations of Ru(IV)−oxo complexes were fixed to be 1.0×10^{-4} M, and the concentration of the substrates was varied from 3.0×10^{-3} to 1.5×10^{-2} M for dihydroanthracene, 3.0×10^{-1} to 1.8 M for ethylbenzene, 5.0×10^{-2} to 5.0×10^{-1} M for cumene, and 5.0×10^{-3} to 4.0×10^{-2} M for cyclohexene. All reactions were conducted under inert atmosphere.

EPR Spectroscopy. EPR spectra were recorded on a JEOL JEXREIXE spectrometer, and g values were determined using an Mn^{2+} marker. ESR spectra were measured at 8 K. A solution were prepared in 0.6 mL of CH_3CN to contain **2** ($[Ru(O)(H^+TPA)(bpy)](PF_6)_3$) (1 mM), cumene (100 mM) and 2,6-lutidine(10 mM) under Ar atmosphere. We confirmed that no Ru(III)−OH were left and alkoxo complex existed by using ESI-MS before measurement.

Electrochemical Measurements. Cyclic voltammetry was employed in acetonitrile in the presence of $TBAPF_6$ (0.1 M) as an electrolyte under Ar at room temperature with use of a glassy carbon electrode as a working electrode, a saturated calomel electrode (SCE) as a reference electrode, and Pt wire as an auxiliary electrode. Cyclic voltammetry in water were also employed with same electrodes in the presence of Na_2SO_4 (0.1 M) as an electrolyte under Ar at room temperature. pH value was adjusted by H_2SO_4. The concentration of **2** (for acetonitrile as solvent) or **2′** ($[Ru(O)(H^+TPA)(bpy)](ClO_4)_3$ for water as solvent) was 1.0 mM and a scan rate was 0.1 V/s.

■ ASSOCIATED CONTENT

Supporting Information. Figures S1−13 and crystallographic data of **2** in the cif format. This material is available free of charge via the Internet at http://pubs.acs.org.

■ AUTHOR INFORMATION

Corresponding Author

kojima@chem.tsukuba.ac.jp; fukuzumi@chem.eng.osaka-u.ac.jp

■ ACKNOWLEDGMENT

This work was supported by Grants-in-Aid (Nos. 21350035, 21750146 and 20108010), a Global COE program, "the Global Education and Research Center for Bio-Environmental Chemistry" from the Japan Society of Promotion of Science (JSPS), the Ministry of Education, Science, Technology of Japan, and by KOSEF/MEST through WCU project (R31-2008-000-10010-0). T.K. also appreciates financial support from The Asahi Glass Foundation.

■ REFERENCES

(1) (a) Sheldon, R. A.; Kochi, J. K. *Metal-Catalyzed Oxidations of Organic Compounds*; Academic Press: New York, 1981. (b) *Activation and Functionalization of Alaknes*; Hill, C. L., Ed.: Wiley: New York, 1989. (c) *The Activation of Dioxygen and Homogeneous Catalytic Oxidation*; Barton, D. H. R., Martell, A. E., Sawyer, D. T., Eds.; Plenum: New York, 1993. (d) Shilov, A. E.; Shul'pin, G. B. *Chem. Rev.* **1997**, *97*, 2879–2932. (e) Meunier, B. *Biomimetic Oxidations Catalyzed by Transition Metal Complexes*; Imperial College Press: London, 1998. (f) Gunay, A.; Theopold, K. H. *Chem. Rev.* **2010**, *110*, 1060–1081.

(2) (a) Dawson, J. H.; Sono, M. *Chem. Rev.* **1987**, *87*, 1255–1276. (b) Sono, M.; Roach, M. P.; Coulter, E. D.; Dawson, J. H. *Chem. Rev.* **1996**, *96*, 2841–2888. (c) Denisov, I. D.; Makris, T. M.; Sliger, S. G.; Schlichting, I. *Chem. Rev.* **2005**, *105*, 2253–2277. (d) Schlichting, I.; Berendzen, J.; Chu, K.; Stock, A. M.; Maves, S. A.; Benson, D. E.; Sweet, R. M.; Ringe, D.; Petsko, G. A.; Sligar, S. G. *Science* **2000**, *287*, 1615–1622.

(3) (a) Wallar, B. J.; Lipscomb, J. D. *Chem. Rev.* **1996**, *96*, 2625–2658. (b) Lippard, S. J. *J. Chem. Soc., Dalton Trans.* **1997**, 3925–3932. (c) Costas, M.; Mehn, M. P.; Jensen, M. P.; Que, L., Jr. *Chem. Rev.* **2004**, *104*, 939–986. (d) Abu-Omar, M. M.; Loaiza, A.; Hontzeas, N. *Chem. Rev.* **2005**, *105*, 2227–2252.

(4) Fe: (a) Hessenauer-Ilicheva, N.; Franke, A.; Meyer, D.; Woggon, W.-D.; van Eldik, R. *J. Am. Chem. Soc.* **2007**, *129*, 12473–12479. (b) Lee, K. A.; Nam, W. *J. Am. Chem. Soc.* **1997**, *119*, 1916–1922. (c) Jackson, T. A.; Rohde, J.-U.; Seo, M. S.; Sastri, C. V.; DeHont, R.; Stubna, A.; Ohta, T.; Kitagawa, T.; Münck, E.; Nam, W.; Que, L. *J. Am. Chem. Soc.* **2008**, *130*, 12394–12407. (d) Chen, K.; Que, L. *J. Am. Chem. Soc.* **2001**, *123*, 6327–6337.

(5) Mn: (a) Fukuzumi, S.; Kishi, T.; Kotani, H.; Lee, Y.-M.; Nam, W. *Nat. Chem.* **2011**, *3*, 38–41. (b) Groves, J. T.; Lee, J.; Marla, S. S. *J. Am. Chem. Soc.* **1997**, *119*, 6269–6273. (c) Pitie, M.; Bernadou, J.; Meunier, B. *J. Am. Chem. Soc.* **1995**, *117*, 2935–2936. (d) Parsell, T. H.; Yang, M.-Y.; Borovik, A. S. *J. Am. Chem. Soc.* **2009**, *131*, 2762–2763. (e) Larsen, A. S.; Wang, K.; Lockwood, M. A.; Rice, G. L.; Won, T.-J.; Lovell, S.; Sadilek, M.; Turecdk, F.; Mayer, J. M. *J. Am. Chem. Soc.* **2002**, *124*, 10112–10123. (f) Wang, K.; Mayer, J. M. *J. Am. Chem. Soc.* **1997**, *119*, 1470–1471. (g) Bryant, J. R.; Taves, J. E.; Mayer, J. M. *Inorg. Chem.* **2002**, *41*, 2769–2776.

(6) Ru:(a) Yip, W.-P.; Yu, W.-Y.; Zhu, N.; Che, C.-M. *J. Am. Chem. Soc.* **2005**, *127*, 14239–14249. (b) Goldstein, A. S.; Beer, R. H.; Drago, R. S. *J. Am. Chem. Soc.* **1994**, *116*, 2424–2429. (c) Thompson, M. S.; Meyer, T. J. *J. Am. Chem. Soc.* **1982**, *104*, 4106–4115. (d) Okumura, T.; Morishima, Y.; Shiozaki, H.; Yagyu, T.; Funahashi, Y.; Ozawa, T.; Jitsukawa, K.; Masuda, H. *Bull. Chem. Soc. Jpn.* **2007**, *80*, 507–517. (e) Lam, W. W. Y.; Man, W.-L.; Leung, C.-F.; Wong, C.-Y.; Lau, T.-C. *J. Am. Chem. Soc.* **2007**, *129*, 13646–13652. (f) Seok, W. K.; Meyer, T. J. *Inorg. Chem.* **2005**, *44*, 3931–3941.

(7) For porphyrin complexes: (a) Groves, J. T.; Nemo, T. E. *J. Am. Chem. Soc.* **1983**, *105*, 6243–6248. (b) Groves, J. T.; Watanabe, Y. *J. Am. Chem. Soc.* **1988**, *110*, 8443–8452. (c) Fujii, H. *J. Am. Chem. Soc.* **1993**, *115*, 4641–4648. (d) Auclair, K.; Hu, Z.; Little, D. M.; Ortiz de Montellano, P. R.; Groves, J. T. *J. Am. Chem. Soc.* **2002**, *124*, 6020–6027.

(8) For nonheme model complexes: (a) Que, L., Jr.; Tolman, W. B. *Angew. Chem., Int. Ed.* **2002**, *41*, 1114–1137. (b) Rohde, J.-U.; In, J.-H.; Lim, M. H.; Brennessel, W. W.; Bukowski, M. R.; Stubna, A.; Münck, E.; Nam, W.; Que, L., Jr. *Science* **2003**, *299*, 1037–1039. (c) Nam, W. *Acc. Chem. Res.* **2007**, *40*, 522–531. (d) Que, L., Jr. *Acc. Chem. Res.* **2007**, *40*, 493–500. (e) Fiedler, A. T.; Que, L., Jr. *Inorg. Chem.* **2009**,

48, 11038–11047. (f) Hirao, H.; Chen, H.; Carvajal, M. A.; Wang, Y.; Shaik, S. *J. Am. Chem. Soc.* **2008**, *130*, 3319–3327. (g) Takahashi, A.; Kurahashi, T.; Fujii, H. *Inorg. Chem.* **2007**, *46*, 6227. (h) Yip, W.-P.; Yu, W.-Y.; Zhu, N.; Che, C.-M. *J. Am. Chem. Soc.* **2005**, *127*, 14239–14249.

(9) (a) Moyer, B. A.; Thompson, M. S.; Meyer, T. J. *J. Am. Chem. Soc.* **1980**, *102*, 2310–2312. (b) Moyer, B. A.; Meyer, T. J. *Inorg. Chem.* **1981**, *20*, 436–444. (c) Che, C.-M.; Yam, V. W.-W.; Mak, T. C. W. *J. Am. Chem. Soc.* **1990**, *112*, 2284–2291. (d) Meyer, T. J.; Huynh, M. H. V. *Inorg. Chem.* **2003**, *42*, 8140–8160. (e) Szczepura, L. F.; Maricich, S. M.; See, R. F.; Churchill, M. R.; Takeuchi, K. J. *Inorg. Chem.* **1995**, *34*, 4198–4205. (f) Dhuri, S. N.; Seo, M. S.; Lee, Y.-M.; Hirao, H.; Wang, Y.; Nam, W.; Shaik, S. *Angew. Chem., Int. Ed.* **2008**, *47*, 3356–3359.

(10) (a) Hirai, Y.; Kojima, T.; Mizutani, Y.; Shiota, Y.; Yoshizawa, K.; Fukuzumi, S. *Angew. Chem., Int. Ed.* **2008**, *47*, 5772–5776. (b) Kojima, T.; Hirai, Y.; Ikemura, K.; Ogura, T.; Shiota, Y.; Yoshizawa, K.; Fukuzumi, S. *Angew. Chem., Int. Ed.* **2010**, *49*, 8449–8453. (c) Lee, Y.-M.; Dhuri, S. N.; Sawant, S. C.; Cho, J.; Kubo, M.; Ogura, T.; Fukuzumi, S. *Angew. Chem., Int. Ed.* **2009**, *48*, 1803–1806. (d) Sawant, S. C.; Wu, X.; Cho, J.; Cho, K.-B.; Kim, S. H.; Seo, M. S.; Lee, Y.-M.; Kubo, M.; Ogura, T.; Shaik, S.; Nam, W. *Angew. Chem., Int. Ed.* **2010**, *49*, 8190–8194.

(11) (a) Lee, Y.-M.; Hong, S.; Morimoto, Y.; Shin, W.; Fukuzumi, S.; Nam, W. *J. Am. Chem. Soc.* **2010**, *132*, 10668–10670. (b) Bryant, J. R.; Mayer, J. M. *J. Am. Chem. Soc.* **2003**, *125*, 10351–10361. (c) Lam, W. W. Y.; Yiu, S. M.; Yiu, D. T. Y.; Lau, T. C.; Yip, W. P.; Che, C. M. *Inorg. Chem.* **2003**, *42*, 8011–8018.

(12) (a) Groves, J. T.; McCluskey, G. A. *J. Am. Chem. Soc.* **1976**, *98*, 859–861. (b) Groves, J. T. *J. Chem. Educ.* **1985**, *62*, 928–931. (c) Sono, M.; Roach, M. P.; Coulter, E. D.; Dawson, J. H. *Chem. Rev.* **1996**, *96*, 2841–2888. (d) Strassner, T.; Houk, K. N. *J. Am. Chem. Soc.* **2000**, *122*, 7821–7822.

(13) Stone, K. L.; Hoffart, L. M.; Behan, R. K.; Krebs, C.; Green, M. T. *J. Am. Chem. Soc.* **2006**, *128*, 6147.

(14) (a) Schoneboom, J. C.; Cohen, S.; Lin, H.; Shaik, S.; Thiel, W. *J. Am. Chem. Soc.* **2004**, *126*, 4017–4034. (b) Sharma, P. K.; de Visser, S. P.; Ogliaro, F. O.; Shaik, S. *J. Am. Chem. Soc.* **2003**, *125*, 2291–2300. (c) de Visser, S. P.; Ogliaro, F. o.; Sharma, P. K.; Shaik, S. *J. Am. Chem. Soc.* **2002**, *124*, 11809–11826. (d) Yoshizawa, K.; Kamachi, T.; Shiota, Y. *J. Am. Chem. Soc.* **2001**, *123*, 9806–9816. (e) Hata, M.; Hirano, Y.; Hoshino, T.; Tsuda, M. *J. Am. Chem. Soc.* **2001**, *123*, 6410–6416.

(15) An oxygen-rebound intermediate has been detected in the peroxynitrite formation by an Fe(IV)-oxo species of myoglobin: Su, J.; Groves, J. T. *J. Am. Chem. Soc.* **2009**, *131*, 12979–12988.

(16) An sulfoxide-bounded complex has been detected by Ru(IV)-oxo species: Roecker, L.; Dobson, J. C.; Vining, W. J.; Meyer, T. J. *Inorg. Chem.* **1987**, *26*, 779–781.

(17) An phenol-bounded complex has been detected by Ru(IV)-oxo species: Seok, W. K.; Dobson, J. C.; Meyer, T. J. *Inorg. Chem.* **1988**, *27*, 3–5.

(18) (a) Kojima, T.; Sakamoto, T.; Matsuda, Y. *Inorg. Chem.* **2004**, *43*, 2245–2247. (b) Kojima, T.; Morimoto, T.; Sakamoto, T.; Miyazaki, S.; Fukuzumi, S. *Chem.—Eur. J.* **2008**, *14*, 8904–8915.

(19) Crystallographic data for **2**: Crystal system orthorhombic, space group *Pbca*, $T = 123$ K, $a = 19.516(4)$ Å, $b = 12.763(2)$ Å, $c = 28.775(5)$ Å, $V = 7167(2)$ Å^3, $Z = 8$, no. of reflections 52108, no. of observations 8201, parameters 528, $R1 = 0.087$ ($I > 2\sigma(I)$), $wR = 0.201$, GOF = 1.24.

(20) (a) Che, C.—M.; Lai, T.—F.; Wong, K.—Y. *Inorg. Chem.* **1987**, *26*, 2289–2299 and references cited therein. (b) Cheng, W.—C.; Yu, W.—Y.; Zhu, J.; Cheung, K.—K.; Peng, S.—M.; Poon, C.—K.; Che, C.—M. *Inorg. Chim. Acta* **1996**, *24*, 105–113. (c) Che, C. M.; Tang, W. T.; Wong, W. T.; Lai, T. F. *J. Am. Chem. Soc.* **1989**, *111*, 9048–9056. (d) Aoyagi, K.; Yukawa, Y.; Shimizu, K.; Mukaida, M.; Takeuchi, T.; Kakihana, H. *Bull. Chem. Soc. Jpn.* **1986**, *59*, 1493–1499.

(21) Evans, D. F.; Jakubovic, D. A. *J. Chem. Soc., Dalton Trans.* **1988**, 2927–2933.

(22) (a) Yamada, H.; Koike, T.; Hurst, J. K. *J. Am. Chem. Soc.* **2001**, *123*, 12775–12780. (b) Paeng, I. R.; Nakamoto, K. *J. Am. Chem. Soc.* **1990**, *112*, 3289.

(23) Luo, Y.-R. *Handbook of Bond Dissociation Energies in Organic Compounds*; CRC Press: Boca Raton, FL, 2003.

(24) Fukuzumi, S.; Ohkubo, K.; Suenobu, T.; Kato, K.; Fujitsuka, M.; Ito, O. *J. Am. Chem. Soc.* **2001**, *123*, 8459–8467.

(25) Griller, D.; Martinho Simões, J. A.; Mulder, P.; Sim, B. A.; Wayner, D. D. M. *J. Am. Chem. Soc.* **1989**, *111*, 7872–7876.

(26) Siu, T.; Picard, C. J.; Yudin, A. K. *J. Org. Chem.* **2005**, *70*, 932–937.

(27) Fujita, M.; Ishida, A.; Takamuku, S.; Fukuzumi, S. *J. Am. Chem. Soc.* **1996**, *118*, 8566–8574.

(28) (a) Wu, A.; Mayer, J. M. *J. Am. Chem. Soc.* **2008**, *130*, 14745–14754. (b) Pan, Z.; Horner, J. H.; Newcomb, M. *J. Am. Chem. Soc.* **2008**, *130*, 7776–7777.

(29) (a) Yoon, J.; Wilson, S. A.; Jang, Y. K.; Seo, M. S.; Nehru, K.; Hedman, B.; Hodgson, K. O.; Bill, E.; Solomon, E. I.; Nam, W. *Angew. Chem., Int. Ed.* **2009**, *48*, 1257–1261. (b) Che, C.-M.; Zhang, J.-L.; Zhang, R.; Huang, J.-S.; Lai, T.-S.; Tsui, W.-M.; Zhou, X.-G.; Zhou, Z.-Y.; Zhu, N.; Chang, C. K. *Chem.—Eur. J.* **2005**, *11*, 7040–7053. (c) Kaizer, J.; Klinker, E. J.; Oh, N. Y.; Rohde, J.-U.; Song, W. J.; Stubna, A.; Kim, J.; Münck, E.; Nam, W.; Que, L. *J. Am. Chem. Soc.* **2004**, *126*, 472.

(30) (a) Bryant, J. R.; Mayer, J. M. *J. Am. Chem. Soc.* **2003**, *125*, 10351–10361. (b) Lam, W. W. Y.; Yiu, S. M.; Yiu, D. T. Y.; Lau, T. C.; Yip, W. P.; Che, C. M. *Inorg. Chem.* **2003**, *42*, 8011–8018.

(31) Stultz, L. K.; Huynh, M. H. V.; Binstead, R. A.; Curry, M.; Meyer, T. J. *J. Am. Chem. Soc.* **2000**, *122*, 5984–5996.

(32) Lebeau, E. L.; Binstead, R. A.; Meyer, T. J. *J. Am. Chem. Soc.* **2001**, *123*, 10535–10544.

(33) In this case, a peak cluster due to a complex bearing an alkoxo ligand derived from oxygenation of anthrone as a precursor of anthraquinone was observed at $m/z = 902.2$ (Figure S8c in the Supporting Information).

(34) Miyazaki, S.; Kojima, T.; Sakamoto, T.; Matsumoto, T.; Ohkubo, K.; Fukuzumi, S. *Inorg. Chem.* **2008**, *47*, 333–343.

(35) Kojima, T.; Hayashi, K.; Shiota, Y.; Tachi, Y.; Naruta, Y.; Suzuki, T.; Uezu, K.; Yshizawa, K. *Bull. Chem. Soc. Jpn.* **2005**, *78*, 2152–2158.

(36) Usually BDEs of O—H bonds in alcohols are more than 90 kcal mol^{-1}: see ref 23.

(37) Bryant, J. R.; Matsuo, T.; Mayer, J. M. *Inorg. Chem.* **2004**, *43*, 1587–1592.

(38) (a) Kojima, T.; Leising, R. A.; Yan, S.; Que, L., Jr. *J. Am. Chem. Soc.* **1993**, *115*, 11328–11335. (b) Mathew, L.; Warkentin, J. *Can. J. Chem.* **1988**, *66*, 11–16. (c) Groves, J. T.; Nemo, T. E. *J. Am. Chem. Soc.* **1983**, *105*, 6243–6248.

(39) Radical species have an extremely short lifetime: Newcomb, M.; Le Tadic-Biadatti, M.-H.; Chestney, D. L.; Roberts, E. S.; Hollenberg, P. F. *J. Am. Chem. Soc.* **1995**, *117*, 12085–12094.

(40) Fokin, A. A.; Schreiner, P. R. *Chem. Rev.* **2002**, *102*, 1551–1593.

(41) (a) Anderegg, G; Wenk, F. *Helv. Chim. Acta* **1967**, *50*, 2330–2332. (b) Gafford, B. G.; Holewerda, R. A. *Inorg. Chem.* **1989**, *28*, 60–66.

(42) Kojima, T.; Amano, T.; Ishii, Y.; Ohba, M.; Okaue, Y.; Matsuda, Y. *Inorg. Chem.* **1998**, *37*, 4076–4085.

(43) Creagh, D. C.; McAuley, W. J. *International Tables for Crystallography*; Wilson, A. J. C., Ed.; Kluwer, Academic Publishers: Boston, 1992; Vol. C, Table 4.2.6.8, pp 219—222.

(44) Ibers, J. A.; Hamilton, W. C. *Acta Crystallogr.* **1964**, *17*, 781.

(45) *CrystalStructyre 3.7.0*: Crystal Structure Analysis Package; Rigaku and Rigaku/MSC: The Woodlands, TX, 2000—2005

(46) Sheldrick, G. M. *SIR 97 and SHELX 97, Programs for Crystal Structure Refinement*; University of Gottingen: Gottingen, Germany, 1997.

(47) We could not determine the positions of the hydrogen atoms of the water molecule of crystallization, which should attach to O2.